Computational Biology and Chemistry 89 (2020) 107398

Contents lists available at ScienceDirect

Computational Biology and Chemistry

journal homepage: www.elsevier.com/locate/cbac

Hit identification against peptidyl-prolyl isomerase of *Theileria annulata* by combined virtual high-throughput screening and molecular dynamics simulation approach

Sezen Spahi [a], Ozal Mutlu [b], Emrah Sariyer [c], Sinem Kocer [d], Erennur Ugurel [a], Dilek Turgut-Balik [a,*]

[a] Yildiz Technical University, Faculty of Chemical and Metallurgical Engineering, Bioengineering Department, Istanbul, Turkey
[b] Marmara University, Faculty of Arts and Sciences, Biology Department, Istanbul, Turkey
[c] Artvin Coruh University, Vocational School of Health Services, Medical Laboratory Techniques, Artvin, Turkey
[d] Istanbul Yeni Yuzyil University, Faculty of Pharmacy, Department of Pharmaceutical Biotechnology, Istanbul, Turkey

ARTICLE INFO

Keywords:
Theileria annulata
Peptidyl prolyl isomerase
Onkogenic signalling patway
Molecular dynamics simulation
Structure-based drug design

ABSTRACT

Theileria annulata secretes peptidyl prolyl isomerase enzyme (*Ta*PIN1) to manipulate the host cell oncogenic signaling pathway by disrupting the tumor suppressor F-box and WD repeat domain-containing 7 (FBW7) protein level leading to an increased level of c-Jun proto-oncogene. Buparvaquone is a hydroxynaphthoquinone anti-theilerial drug and has been used to treat theileriosis. However, *Ta*PIN1 contains the A53 P mutation that causes drug resistance. In this study, potential *Ta*PIN1 inhibitors were investigated using a library of naphthoquinone derivatives. Comparative models of mutant (m) and wild type (wt) *Ta*PIN1 were predicted and energy minimization was followed by structure validation. A naphthoquinone (hydroxynaphthalene-1,2-dione, hydroxynaphthalene-1,4-dione) and hydroxynaphthalene-2,3-dione library was screened by Schrödinger Glide HTVS, SP and XP docking methodologies and the docked compounds were ranked by the Glide XP scoring function. The two highest ranked docked compounds Compound 1 (4-hydroxy-3-[3,4,5-trihydroxy-6-(hydroxymethyl)oxan-2-yl]oxynaphthalene-1,2-dione) and Compound 2 (6-acetyl-1,4,5,7,8-pentahydroxynaphthalene-2,3-dione) were used for further molecular dynamics (MD) simulation studies. The MD results showed that ligand Compound 1 was located in the active site of both m*Ta*PIN1 and wt*Ta*PIN1 and could be proposed as a potential inhibitor by acting as a substrate antagonist. However, ligand Compound 2 was displaced away from the binding pocket of wt*Ta*PIN1 but was located near the active site binding pocket of m*Ta*PIN1 suggesting that could be selectively evaluated as a potential inhibitor against the m*Ta*PIN1. Compound 1 and Compound 2 ligands are potential inhibitors but Compound 2 is suggested as a better inhibitor for m*Ta*PIN1. These ligands could also further evaluated as potential inhibitors against human peptidyl prolyl isomerase which causes cancer in humans by using the same mechanism as *Ta*PIN1.

1. Introduction

Theileria annulata is a tick-borne parasite which causes tropical theileriosis in cattle (Viseras et al., 1999). The disease threatens about 250 million cattle (Abdul-Husin et al., 2016) and causes financial losses worldwide (Sudan et al., 2017). Both symptomatic and subclinical conditions are observed among infected animals such as weight loss, decreased milk yield, miscarriage and in some cases deaths (Gharbi and Darghouth, 2015).

Among the Apicomplexa parasites, *Theileria* genus has the ability to transform host cells causing uncontrolled proliferation, cellular migration and metastasis, resistance to apoptosis, resulting in malignant phenotype formation (Woods et al., 2013). In 2015 J. Marsolier et al. identified a human PIN1 homolog in *T. annulata* that is use to manipulate of host oncogenic signaling pathway by disrupting the balance of tumor suppressor F-box and WD repeat domain-containing 7 (FBW7) (Marsolier et al., 2015). Ubiquitin ligase complex of SKP1, CUL1 and F-box protein containing FBW7 substrate recognition member (SCF

* Corresponding author at: Yildiz Technical University, Faculty of Chemical and Metallurgical Engineering, Department of Bioengineering, Davutpasa Campus, 34210, Esenler, Istanbul, Turkey.
E-mail address: dilekbalik@gmail.com (D. Turgut-Balik).

https://doi.org/10.1016/j.compbiolchem.2020.107398
Received 25 May 2020; Received in revised form 7 September 2020; Accepted 29 September 2020
Available online 2 October 2020

^{FBW7}), degrades some of the proto-oncogenes functioning in the pathways of cellular growth and division including, cyclin E, Notch, MYC and JUN (Welcker and Clurman, 2008). Dimerization of FBW7 enhances substrate activity of many SCF E3 ligase complexes and also contributes to the stabilization of FBW7 level in the cells by supporting *trans*--autoubiquitylation of FBW7 (Welcker et al., 2013).

Human PIN1 recognizes the phospho serine or threonine peptide sequence that precedes to proline (pSer / Thr-Pro) in particular (Yaffe et al., 1997). FBW7 is a PIN1 substrate that contains the PIN1 binding site pThr205-Pro near conserved dimerization domain. PIN1 causes conformational change by binding to FBW7 and disrupts dimerization of FBW7 leading to enhance auto-ubiquitination (Min et al., 2012). *Ta*PIN1 uses this ability to promote tumor-like phenotype in parasitized host cells by destabilization of FBW7 which indirectly enhances the cellular levels of c-Jun proto-oncogene (Marsolier et al., 2015).

Host cell phenotypic transformation can be reversed by treatment of a single injection of buparvaquone at 2.5 or 5 mg/kg (McHardy et al., 1985). However, Marsolier et al. (2015) reported that *Ta*PIN1 is mutated (A53 P substitution) in buparvaquone resistant theileriosis emerging clinical concern for the cattle along infected areas (Marsolier et al., 2015). This resistance was confirmed by a recent study conducted on *T. annulata* parasites isolated in Sudan (Salim et al., 2019).

The development of new drugs with traditional methods take many years and cost about $ 2.6 billion, including the cost of failure (Mullard, 2014). Computer-aided drug design (CADD) has gained great importance in the process of new drug discovery and development due to the reduced time and cost requirements (Cerqueira et al., 2015). CADD provides an early evaluation of selectivity and activity of lead candidates, as well as their pharmacological effects and toxicity. The basis of the approach is the application of computational techniques that facilitate and accelerate the discovery of new molecular entities (Song et al., 2009). Computer-aided drug design approaches are divided into two sections, structure-based and ligand-based methods (Macalino et al., 2015). The structure-based drug design (SBDD) approach involves the use of target molecule (enzyme/receptor) 3D structure for the screening or generation of potential ligands (Macalino et al., 2015). Accordingly, SBDD approach is believed to be more sufficient and is widely used in academic laboratories (Zhang et al., 2016). Furthermore, molecular docking-based virtual screening and MD simulation are among the most commonly used SBDD strategies because of their broad range of applications in the analysis of molecular recognition events like in molecular interactions and binding energy (Ferreira et al., 2015; Kalyaanamoorthy and Chen, 2011).

Buparvaquone is a hydroxynaphthoquinone antiprotozoal drug (Hashemi-Fesharki, 1991) and this may suggest that other naphthoquinone derivatives could also be effective on *Theileria* parasites. In this study, potential inhibitors against drug-resistant *Ta*PIN1 (m*Ta*PIN1) and wild type *Ta*PIN1 (wt*Ta*PIN1) was investigated using a naphthoquinone (hydroxynaphthalene-1,2-dione, hydroxynaphthalene-1,4-dione) and hydroxynaphthalene-2,3-dione library by structure-based drug design approches including homology modeling, virtual screening and MD simulation.

2. Materials and methods

2.1. Homology model building of mutant and wild type TaPIN1

Homology models of mutant and wild type *Ta*PIN1 were predicted using the amino acid sequence of *Theileria annulata* peptidyl prolyl isomerase (NCBI accession number TA18945) (Pain et al., 2005). The original amino acid sequence of the enzyme was changed to reveal A53 P mutation to mimic buparvaquone resistant mutant *Ta*PIN1 coding sequence.

Structural template was selected using NCBI BLAST server and PSI-BLAST (Position-Specific Iterative Basic Local Alignment Search Tool) search (https://blast.ncbi.nlm.nih.gov). Structure with the highest max score, the lowest E-value and the highest % identity score was selected as a template for homology modeling and retrieved from the RCSB PDB database (https://www.rcsb.org). Three-dimensional structures of mutant and wild type *Ta*PIN1 were built by using MODELLER v9.15 software (Eswar et al., 2006) and the best models were selected according to DOPE score among 50 models. Energy minimization of the selected mutant and wild type protein models was performed by using AMBER 14SB forcefield (Maier et al., 2015) and applying 2000 steps of Steepest Descent algorithm (Fletcher and Powell, 1963). Superimposition was carried out by Chimera v1.10.2 software (Pettersen et al., 2004). Optimized protein models were subjected to quality validation steps by several types of servers including ERRAT v2.0 (Colovos and Yeates, 1993), ProQ (Wallner and Elofsson, 2003), ProSa (Wiederstein and Sippl, 2007) and Rampage (Lovell et al., 2003).

2.2. High-throughput virtual screening and molecular docking

High-throughput virtual screening and molecular docking were performed using Glide (Schrödinger Release 2017-1: Glide, Schrödinger, LLC, New York, NY, 2017) program in Schrödinger Maestro 2017.1 (Schrödinger Release 2017-1: Maestro, Schrödinger, LLC, New York, NY, 2017). Protein Preparation Wizard (Schrödinger Release 2017-1: Protein Preparation Wizard, Schrödinger, LLC, New York, NY, 2017) module was used to add missing hydrogen atoms, minimize structure and assign protonation state by PROPKA at pH7.0 for m*Ta*PIN1 and wt*Ta*PIN1 structures. The binding site of each predicted structure was defined by the Receptor Grid Generation module.

The ligand library containing 2979 naphthoquinone (hydro xynaphthalene-1,2-dione, hydroxynaphthalene-1,4-dione) and hydroxynaphthalene-2,3-dione derivatives was retrieved from the PubChem database (Kim et al., 2015). Prior to docking, all ligands were prepared by using LigPrep (Schrödinger Release 2017-1: LigPrep, Schrödinger, LLC, New York, NY, 2017). Ligand preparation was performed to predict 3-dimensional structure and energy minimization by applying OPLS3 forcefield (Harder et al., 2015).

All compounds were docked into the active site of both wild type and mutant protein structure by applying Glide HTVS (High throughput virtual screening), SP (Standard precision) and XP (Extra precision) docking methods respectively (Friesner et al., 2004, 2006). At the end of the docking procedure, poses were ranked according to XP Glide Score which is defined as follows (Friesner et al., 2006).

XP GlideScore = Ecoul + EvdW + Ebind + Epenalty

Ebind = Ehyd_enclosure + Ehb_nn_motif + Ehb_cc_motif + EPI + Ehb_pair + Ephobic_pair

Epenalty = Edesolv + Eligand_strain

Drug-likeness of selected compounds were predicted by using QikProp (QikProp, Schrödinger, LLC, New York, NY, 2017).

2.3. MM/GBSA binding free energy calculations of hit compounds

The MM-GBSA dG binding energy of the hit compounds was estimated by using Prime program (Schrödinger Release 2017-1: Prime, Schrödinger, LLC, New York, NY, 2017). The binding energy was calculated by the software according to the following equation.

ΔG = E_complex (minimized) - (E_ligand (minimized) + E_receptor (minimized))

2.4. Molecular dynamics simulation

2.4.1. Molecular dynamics simulation for mutant and wild type TaPIN1 homology models

MD simulation was performed for the homology models of both m*Ta*PIN1 and wt*Ta*PIN1 using AMBER ff14SB force field (Maier et al., 2015). The systems were solvated with TIP3PBOX (Mark and Nilsson, 2001) water molecules in an octahedral box size 10 Å and then was neutralized by adding Cl^- and Na^+ ions. The energy minimization of the

systems was carried out with 1000 steps of Steepest Descent (Fletcher and Powell, 1963). followed by 9000 steps of conjugate gradient algorithms (Møller, 1993). After minimization, Langevin thermostat (Davidchack et al., 2009) with a collision frequency of $\gamma = 10.0\ ps^{-1}$ was employed to heat systems from 10 K to 300 K with constant volume and pressure. MD simulations were performed for 50 ns with a time step of 2 fs and SHAKE algorithm (Ryckaert et al., 1977) was applied to restraint all atoms during dynamics run. The temperature was controlled using Berendsen the weak-coupling algorithm (Berendsen et al., 1984) during MD simulation.

2.4.2. Molecular dynamics simulation for docked complexes

The dynamic behavior of the two highest ranked docked complexes were studied by MD simulation using the general AMBER force field (gaff) (Sprenger et al., 2015) with AM1-BCC charge model (Jakalian et al., 2002). Topology and coordinate files of the docked complexes were prepared using AMBER tLEaP (Salomon-Ferrer et al., 2013) cpp, and energy minimizations were carried out as in systems of the native proteins to remove bad contact and clash. Following energy minimizations, systems of the two highest ranked docked complexes were simulated during 100 ns, at 300 K, constant volume and pressure.

MD simulation trajectory files of each type of *Ta*PIN1 predicted models and the two highest ranked docked complexes were analyzed using CPPTRAJ (Roe and Cheatham, 2013). Root-mean square deviation (RMSD) and root-mean square fluctuation (RMSF) of the C_α backbone carbon atoms were plotted using GNUPLOT software (Janert, 2010).

3. Results

3.1. Homology modeling and validation of mutant and wild type TaPIN1

Three-dimensional models of m*Ta*PIN1 and wt*Ta*PIN1 enzymes were predicted by using NMR spectroscopy solution structure of the peptidyl prolyl isomerase (PPIase) domain of human Pin1 (hPIN1) as a template (PDB ID: 1NMW) (Bayer et al., 2003). According to the PSI-BLAST search results, wt*Ta*PIN1 and PPIase domain of hPIN1 has 47 % sequence identity with the E- value of 9e-30, and a max score of 104. Fifty different models were generated for each type of proteins by MODELLER v9.15 software and the best models were chosen for m*Ta*PIN1 and wt*Ta*PIN1 with the lowest DOPE score of -11874.99805 and -11530.91309, respectively. Energy minimization of both types of *Ta*PIN1 was performed and modeled structures were superimposed with template PPIase domain of the hPIN1 protein. The average root mean square deviation (RMSD) values for m*Ta*PIN1 and wt*Ta*PIN1 (0.502 Å and 0.479 Å respectively) displayed quite similarities with the template protein. Both models were subjected to structure validation steps by using ERRAT v2.0 (Colovos and Yeates, 1993), ProQ (Wallner and Elofsson, 2003), ProSa (Wiederstein and Sippl, 2007) and Rampage (Lovell et al., 2003) (Table 1). m*Ta*PIN1 and wt*Ta*PIN1 predicted structures have ERRAT overall quality factor of 86.325 and 81.148, respectively. After the minimization, most amino acid residues of both models observed within the 95 % confidence limits according to ERRAT results. According to ProSA results, Z scores of mutant and wild type models were found −3.3 and −3.19, respectively. These scores were located within the range of scores among NMR solvated native proteins structures. Peptidyl prolyl isomerase (PPIase) domain of human Pin1 (hPIN1) (PDB ID: 1NMW) was selected as template protein and the template is a native protein that was experimantally analyzed by NMR spectroscopy. Therefore, the results showed that these models were generated at accaptable accuracy. When the energy graph was examined, the multiplicity of residues in the negative region indicates that the conformations of the modeled proteins were correctly determined. The expectation of the residue percentage in the favored region from the Ramachandran diagram of a good model was accepted as 90 % and above (Mahgoub and Bolad, 2013). The percentages of residues in the favored region were 91.4 % and 90 % respectively for the m *Ta*PIN1 and wt*Ta*PIN1 models. LGscore obtained from ProQ server were 2.759 for wt*Ta*PIN1 model and 2.261 for m*Ta*PIN1 model. According to LGscores, wt*Ta*PIN1 model was built as very good model (LGscore> 2.5 is very good model) and m*Ta*PIN1 model was predicted as good model (LGscore> 1.5 is fairly good model) (Wallner and Elofsson, 2003). Collectively, all these validation results confirmed that the enzymes were modeled with high accuracy and a reliable model. All graphs obtained from validation were given in Supplementary Figs. 1–3.

3.2. High-throughput virtual screening and molecular docking

The virtual library was docked initially to the active site of m*Ta*PIN1 by using GLIDE HTVS, SP and XP docking methods, respectively, and poses were ranked based on XP GScores (Table 2). Then selected top 10 ligands based on XP GScores were also docked to wild-type enzyme for comparision (Table 2). Buparvaquone was also docked to the active site of both types of enzymes and compared with hit compounds for control (Table 2). The compound 1 was the best ranking ligand based on XP GScore and MM-GBSA free energy calculations on both mutant and wild-type enzymes. Compound 1 had −7.789 kcal/mol and −8.176 kcal/mol XP GScores on m*Ta*PIN1 and wt*Ta*PIN1, respectively, while the ΔG binding energies were −39.319 kcal/mol and −42.328 kcal/mol based on the MM-GBSA calculation method. Hydrogen-bond contributions were not so different in both interactions. The most striking results were taken from compound 2 which had -20.159 kcal/mol and 3.918 kcal/mol ΔG binding energies, and −7.680 and −7.162 kcal/mol of XP GScores on the mutant and wild type structures, respectively. The XP GScore and ΔG binding energies of compound 2 in mutant structure were lower than the wild-type. Therefore, binding affinity of the compound to the mutant structure is visibly higher than the wild-type structure. The best pose of the buparvaquone had the highest XP GScores (XP GScores −3.574 kcal/mol and −4.497 kcal/mol, in mutant and wild-type, respectively) when compared with the other hit compounds. Moreover, docking score and ΔG binding energies of the buparvaquone for wild-type were better than the mutant one, which showed consistency with the results of the *in vitro* assays (Table 2) (Marsolier et al., 2015).

The *Ta*PIN1 catalytic residues were determined as His34, Cys92, His136, Lys38 and Arg43 by reference to the catalytic residues in human PIN1 (Daum et al. (2006); Velazquez and Hamelberg (2013), Schiene--Fischer (2015). According to the docking results, it was observed that compound 1 interacted with the Lys38, Asn47, and Asn44; compound 2 interacted with Lys38, Asn47, Ser133, and Ser93; buparvaquone interacted with Lys38 residues of m*Ta*PIN1 (Fig. 1a,b,c). In mutant structure, all of the residues except Lys38 interacted with ligands formed hydrogen bond but Lys38 formed a salt bridge with ligands. Docking results

Table 1
Validation scores of m*Ta*PIN1 and wt*Ta*PIN1 predicted structures.

Protein Models	Web-Server					
	ERRAT (Overall quality factor)	ProSA (Z-score)	ProQ (LGscore)	RAMPAGE (Ramachandran plot) Favored region (%)	Allowed region (%)	Outlier region (%)
m*Ta*PIN1	86.325	−3.3	2.261	91.4	8.6	0.0
wt*Ta*PIN1	81.148	−3.19	2.759	90	7.1	2.9

Table 2
Molecular docking output of top 10 hit compounds against m*Ta*PIN1 and wt*Ta*PIN1.

Compound numbers	Name	Mutant *Ta*PIN1			Wild type *Ta*PIN1		
		XP GScore (kcal/mol)	XP Hbond (kcal/mol)	MMGBSA ΔG (kcal/mol)	XP GScore (kcal/mol)	XP Hbond (kcal/mol)	MMGBSA ΔG (kcal/mol)
Compound 1	4-hydroxy-3-[3,4,5-trihydroxy-6-(hydroxymethyl) oxan-2-yl]oxynaphthalene-1,2-dione	−7.789	−2.243	−39.319	−8.176	−2.144	−42.328
Compound 2	6-acetyl-1,4,5,7,8-pentahydroxynaphthalene-2,3-dione	−7.680	−0.157	−20.159	−7.162	−1.756	3.918
Compound 3	3-butanoyl-4,5,7-trihydroxynaphthalene-1,2-dione	−7.501	−1.007	−20.465	−4.831	−2.159	−34.740
Compound 4	6-ethyl-4,5,7,8-tetrahydroxynaphthalene-1,2-dione	−7.453	−1.642	−1.899	−5.906	−1.172	−6.110
Compound 5	6-ethyl-1,4,5,7-tetrahydroxynaphthalene-2,3-dione	−7.223	−1.397	−17.648	−6.628	−1.047	−7.860
Compound 6	3,6-diacetyl-4,5,7,8-tetrahydroxynaphthalene-1,2-dione	−7.139	−1.808	−15.740	−6.758	−1.890	−7.047
Compound 7	7-acetyl-1,5,6,8 tetrahydroxynaphthalene-2,3-dione	−6.931	−1.310	−11.941	−5.091	−0.906	−7.551
Compound 8	2-(2-acetyl-3-hydroxycyclohex-2-en-1-yl)-8-hydroxynaphthalene-1,4-dione	−6.648	−1.810	−37.525	−5.104	−1.090	−34.238
Compound 9	4,5,6,8-tetrahydroxynaphthalene-1,2-dione	−6.574	−1.059	−8.724	−6.967	−2.081	−23.137
Compound 10	4,5,6,7,8-pentahydroxy-3-methoxynaphthalene-1,2-dione	−6.572	−0.680	−23.048	−6.601	−2.304	−26.971
71768 (Pubchem)	Buparvaquone	−3.574	−0.391	−29.92	−4.497	−0.700	−32.49

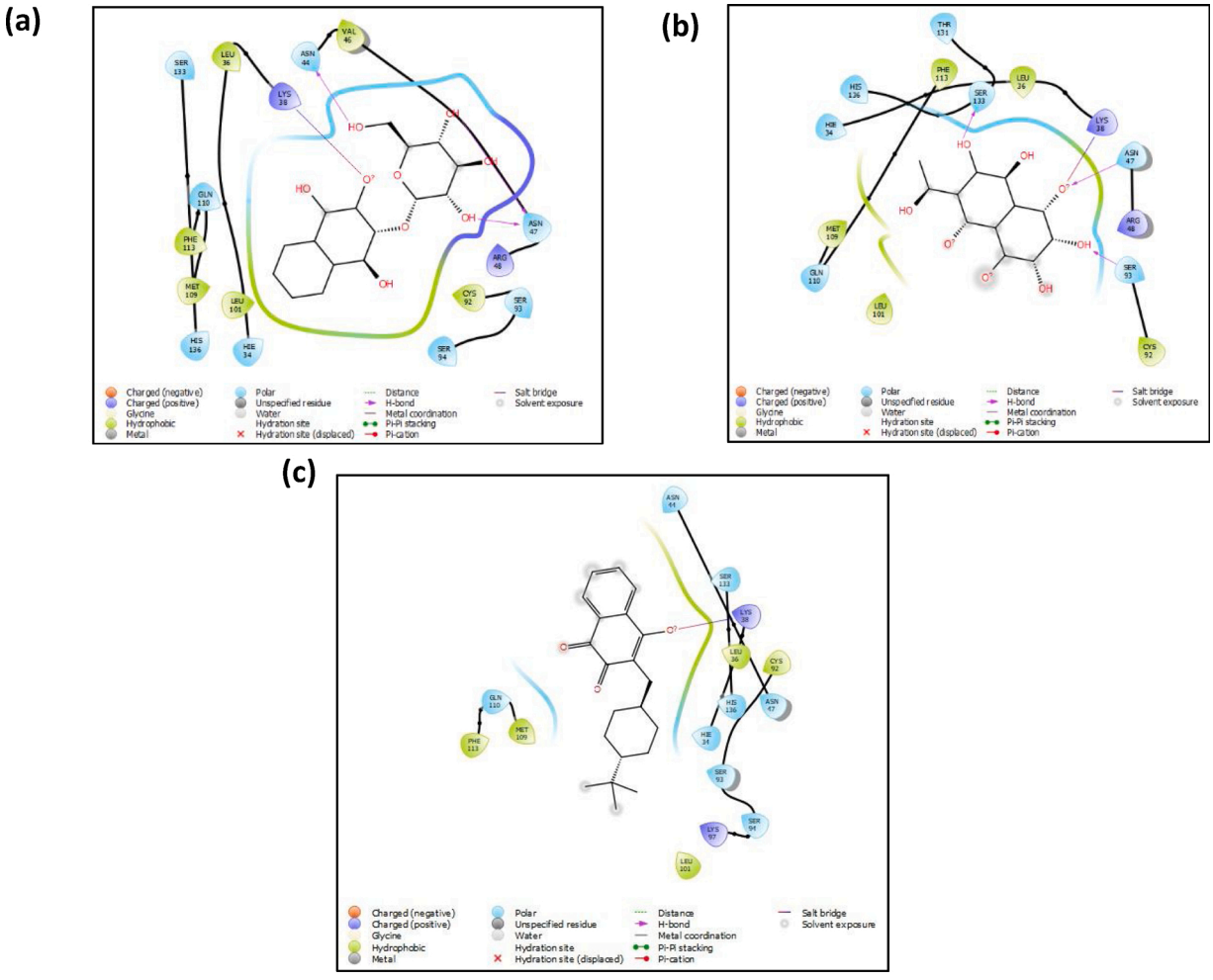

Fig. 1. Molecular interactions of m*Ta*PIN1 with (a) Compound 1, (b) Compound 2 and (c) Buparvaquone.

showed that the compound 1, compound 2 and buparvaquone interacted with the active site residue (Lys38) only in the mutant enzyme. Besides, compound 1 interacted with Asn47, Asn44, Val46 and Ser133; compound 2 interacted with Asn47, Ser133, Ser93 and Gln110; buparvaquone interacted with Asn47 and Ser133 residues of wt*Ta*PIN1 (Fig. 2a, b,c).

Physicochemical properties of the compounds depend to their structure they have. Therefore, slight modifications in the structures will result with improved properties. In our study, hit compounds were analysed for their drug-like features. All hit compounds obey the Lipinski's rule of five. However Caco-2 cell wall permeability and human oral absorption of most hits were low due to their low Log*Po/w* values. So, lead optimization towards cellular permeability should be done for the hits. Plog values for hERG channel blocking and serum albumin binding were found to be in reference ranges (Table 3).

3.3. Molecular dynamics simulation

MD simulation studies were performed for ligand-free *Ta*PIN1 and ligand-*Ta*PIN1 complexes for the further analysis of conformational changes in ligand-induced receptor structures and evaluation of the stability of ligand-receptor complex structures. Stability of the systems and deviation between the positions were evaluated using the RMSD and root mean square fluctuation (RMSF) values subtracted from MD simulation trajectory during 50 ns and 100 ns for ligands free *Ta*PIN1 and ligand-*Ta*PIN1 complexes of both wild and mutant type enzymes respectively.

Residues between 1–30 of mutant and wild type enzymes were ignored because they do not fold a secondary structure causing an increase of RMSD value unnecessarily. The average RMSD value of ligand-free m*Ta*PIN1 and wt*Ta*PIN1 were calculated as 2.107 Å and 2.572 Å, respectively (Fig. 3a). C_α fluctuation of residues of both enzymes was the same as the region between 40–50 and 70–80 in the RMSF plot but the mutant type enzyme was found to be more rigid than the wild type enzyme (Fig. 3b). Due to the A53 P mutation, the α-helix secondary structure had formed in the 40–55 region of the mutant enzyme and therefore became more rigid in the structure. The changes appeared to indirectly caused more displacement of the α-helix region between residues 60–80.

The average RMSD value of the Compound 1-m*Ta*PIN1 complex was calculated as 2.070 Å and the minor deviations were observed along 100 ns MD simulation (Fig. 3c). RMSD value of Compound 2–m*Ta*PIN1 complex was observed increasing gradually up to about 55 ns until reaching equilibrium and stabilized with an average RMSD value of 2.416 Å at 55−100 ns period (Fig. 3c).

RMSD value of Compound 1-wt*Ta*PIN1 complex was observed rising up to 55 ns and then stabilized at 55−100 ns period with the average RMSD value of 3.706 Å (Fig. 3c), but it was observed that RMSD value of Compound 2–wt*Ta*PIN1 complex structure remained constant at 3 Å until 80 ns and suddenly rose for 80−95 ns period then became stable with average RMSD value of 3.219 Å (Fig. 3c).

In the RMSF graph, the fluctuations between 1–30 residues of proteins resulted from the fact that there is no secondary structure in that region (Fig. 3d). Significant fluctuations were observed between

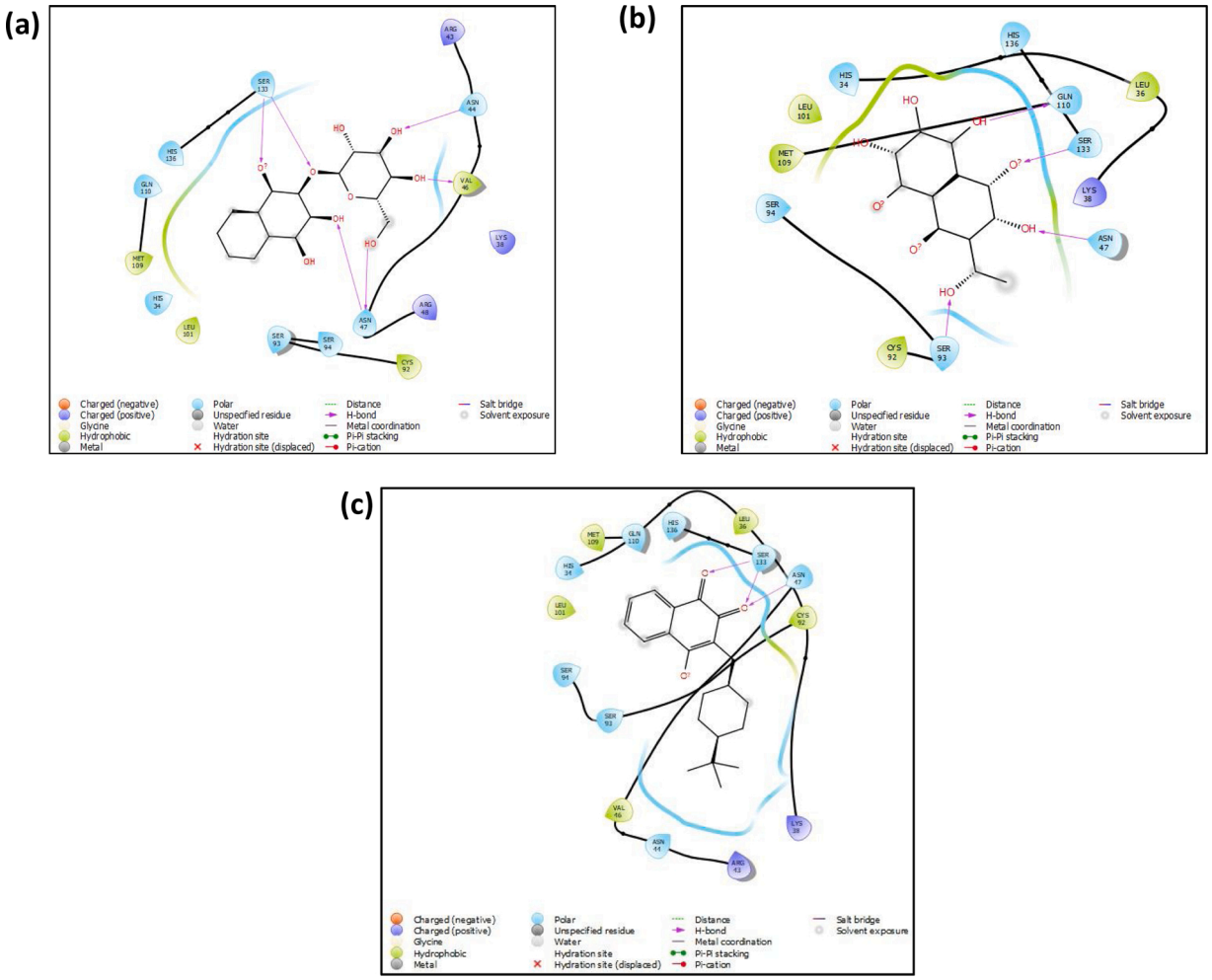

Fig. 2. Molecular interactions of wt*Ta*PIN1 with (a) Compound 1, (b) Compound 2 and (c) buparvaquone.

Table 3
Drug-like properties of resultant hit compounds.

Properties	Compounds										Reference ranges (for 95 % of known drugs)
	Compound 1	Compound 2	Compound 3	Compound 4	Compound 5	Compound 6	Compound 7	Compound 8	Compound 9	Compound 10	
MW	352.297	280.190	276.245	250.207	250.207	306.228	264.191	312.321	222.154	268.179	(130.0 / 725.0)
PSA	177.327	175.796	136.835	131.376	134.423	180.581	159.875	119.806	137.319	161.423	(7.0 / 200.0)
NROTB	8	6	6	5	5	6	5	3	4	6	(0.0 / 15.0)
HBD	5	3	2	3	4	0	2	0	2	4	(0.0 / 6.0)
HBA	14	7.75	7.25	6	7	7	7	5.5	5	7.5	(2.0 / 20.0)
Log*Po/w*	−1.739	−1.286	0.028	−0.286	−0.777	−0.560	−0.876	1.594	−0.612	−1.234	(-2.0 / 6.5)
Log*S*	−1.643	−1.547	−2.187	−1.788	−1.696	−1.218	−1.616	−2.960	−1.364	−1.323	(-6.5 / 0.5)
Log*K* HSA	−1.067	−0.764	−0.604	−0.594	−0.690	−0.990	−0.712	−0.229	−0.647	−0.771	(-1.5 / 1.5)
PermCaco-2	31	7	49	46	37	11	13	132	24	18	(<25 poor, >500 high)
PlogHERG	−4.388	−3.557	−4.235	−3.642	−3.619	−3.902	−3.637	−4.220	−3.449	−3.279	(concern below −5)
%HumanOralAbsorption	44	35	58	55	51	42	42	74	48	52	(<25 poor, >500 high)
Lipinski's violations	0	0	0	0	0	0	0	0	0	0	(maximum is 4)

MW: molecular weight; PSA: vdW polar surface area; NROTB: number of rotatable bonds; HBD: number of hydrogen bond donors; HBA: number of hydrogen bond acceptors; LogPo/w: predicted octanol/water partition coefficient; LogS: predicted aqueous solubility; LogK HSA: prediction of binding to human serum albumin; PermCaco-2: Predicted apparent Caco-2 cell permeability in nm/sec; PlogHERG: Predicted IC50 value for blockage of HERG K+channels; %Human Oral Absorption: Predicted human oral absorption on 0–100% scale.

100–120 residues of both ligand-wt*Ta*PIN1 complexes when the RMSF results of ligand-free and ligand-bound wtTaPIN1 were compared (Fig. 3d). The region having much more fluctuation during 100 ns was the α-helix structure around the region of active pocket and ligand binding site. Besides, the region between 40–50 and 70–80 showed more fluctuation according to RMSF plot.

In the presence of Compound 1 lead compound, fluctuations were observed between residues 45–55 of m*Ta*PIN1, but none of the important fluctuations were observed in the presence of Compound 2 lead compound (Fig. 3d). The m*Ta*PIN1 generally has a more stable structure than wt*Ta*PIN1 but the 45–55 region shows high fluctuation in the Compound 1-m*Ta*PIN1 complex.

The interaction between Compound 1 lead compound and m*Ta*PIN1 was stable according to superimposition before and after simulation results (Fig. 4a). After the simulation, ligand Compound 1 was observed to remain its interaction with catalytic residues of m*Ta*PIN1 as in the first position, but also stable interactions with Lys38 according to the first position. Besides, the interactions of Compound 1 with Glu91, Ser93 and Ser133 were formed. However, lead compound Compound 2 was observed to change its initial position after 100 ns MD simulation with m*Ta*PIN1 (Fig. 4b) and lost many interactions but formed three hydrogen bonds with Arg48, Lys38 and Ser93.

After MD running of Compound 1-wt*Ta*PIN1 complex structure, Compound 1 ligand was observed to lost all hydrogen bonding interactions according to its first position but formed hydrogen bonding interaction with two residues (Gln110, Leu101) that differ than the interaction in the first position (Fig. 4c). Furthermore, Compound 2 ligand showed no catalytic residue interactions with wt*Ta*PIN1 (Fig. 4d), but the interaction of wt*Ta*PIN1 with Lys97 and Arg96 were hydrogen bonding interactions. Accordingly, these results suggest that Compound 2 compound almost totally displaced of the initial region of the wt*Ta*PIN1.

4. Discussion

In this study, for the first time in the literature, molecular docking studies of mutant and wild type *Ta*PIN1 enzymes with compounds composed of naphthoquinone derivatives were carried out to determine potential inhibitor candidates. After moleculer docking of mutant *Ta*PIN1 enzyme with 2979 naphthoquinone derivatives according to XP GScores top 10 ligands were selected as hit compounds and also docked to wild type enzyme for comparision. Buparvaquone was also docked to the active site of both types of enzymes and compared with hit compounds for control.

XP GScore and free energy of binding (MM/GBSA) calculations of docking results showed that the most potent ligand on both enzymes was compound 1. Furthermore, compound 2 also showed good binding affinity on mutant structure and the free-energy of binding was much lower than the wtTaPIN1. Therefore these two ligands were selected as lead compounds for MD simulation analyses.

As a result of the MD simulation studies with two lead ligands, the Compound 1 ligand was observed to be stable in the active site of both wild type and the mutant *Ta*PIN1 enzymes and was predicted as a potential inhibitor. However, Compound 2 ligand was observed to be located outside the active site of the wt*Ta*PIN1 and was not stable, but the ligand was observed to interact with catalytic residues near the active site of the m*Ta*PIN1. Accordingly, ligand Compound 2 could be evaluated as a most potential inhibitor for the m*Ta*PIN1.

5. Conclusions

Buparvaquone is a hydroxynaphthoquinone drug used in the treatment of theileriosis (Hashemi-Fesharki, 1991). However, the identification of some mutations causing drug resistance (Marsolier et al., 2015; Sharifiyazdi et al., 2012) requires urgent determination of alternative inhibitors. In this study, we applied structure-based drug design to

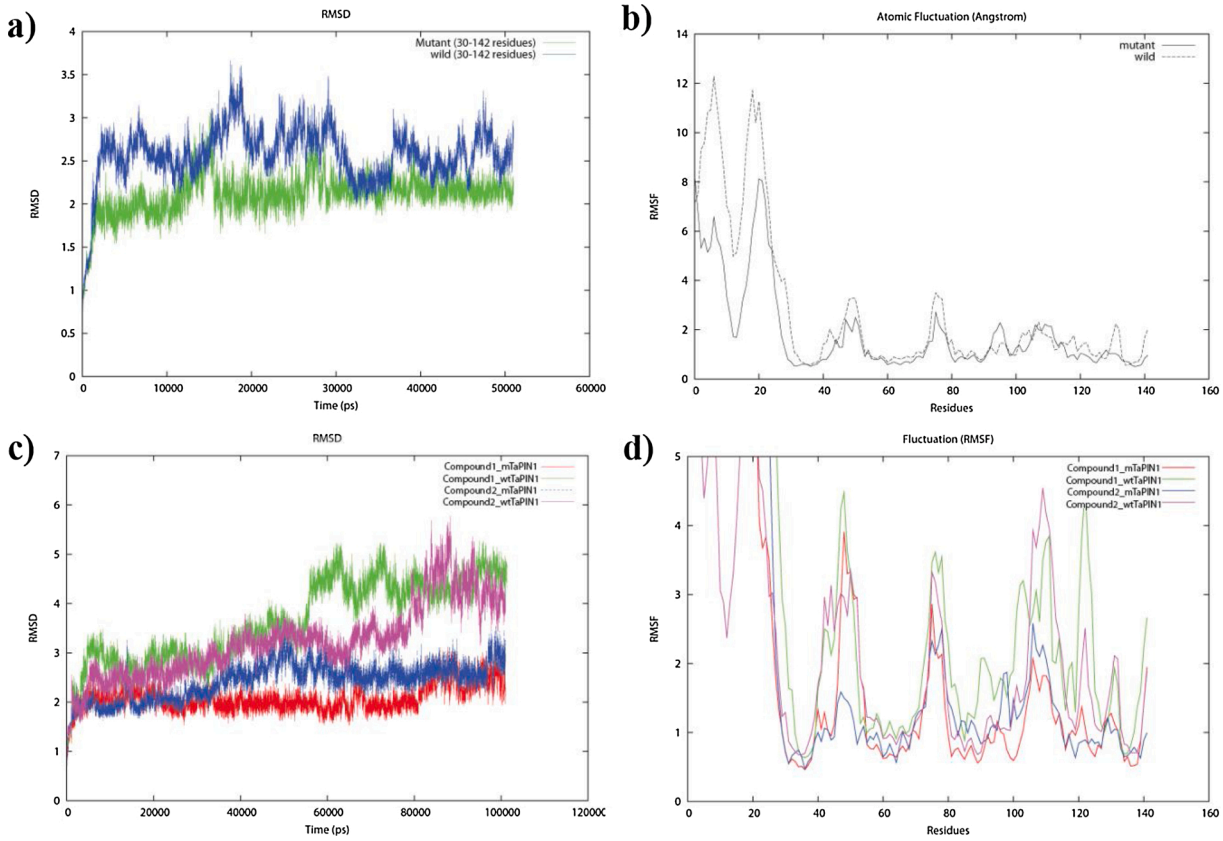

Fig. 3. a) RMSD (average C_α backbone deviation) graph of ligands free proteins b) The RMSF values (C_α backbone fluctuation of each residue) of ligands free proteins c) RMSD (average C_α backbone deviation) graph of ligands-*Ta*PIN1 complex d) RMSF (C_α backbone fluctuation of each residue) values of ligands-*Ta*PIN1 complex during MD simulation.

discover new inhibitors against m*Ta*PIN1 and wt*Ta*PIN1. According to molecular docking studies, two compounds (compound 1 and 2) with the lowest XP GScores among the naphthoquinone derivatives were selected and simulated with mutant and wild-type enzymes using molecular dynamics methods. Furthermore, ligands 1 and 2 showed lowest docking energies on m*Ta*PIN1 structure than the buparvaquone.

Compound 1 ligand-bound mutant *Ta*PIN1 enzyme MD simulation studies showed that ligand appears te be bound to the active site of the mutant enzyme and remains stable for 100 ns. Furthermore, according to Compound 1 ligand-bound wild type *Ta*PIN1 enzyme MD simulations studies, the ligand was located in the active site of wild type enzyme during simulation. So, Compound 1 can be recommended as an inhibitor against both type of *Ta*PIN1 enzymes.

According to Compound 2 ligand bound m*Ta*PIN1 MD simulation studies, it was observed that Compound 2 ligand interacts with catalytic residues near the active site of the m*Ta*PIN1. Accordingly, ligand Compound 2 could be evaluated as a potential inhibitor for the m*Ta*PIN1 enzyme. However, according to Compound 2 ligand-bound wt*Ta*PIN1 MD studies, Compound 2 was located outside of the active site binding pocket of the wt*Ta*PIN1 enzyme. Since the 3-D structure of the mutant enzyme was more rigid than the wild-type enzyme, its interaction with the buparvaquone enzyme had been more weakness.

These results suggest that the ligands could be evaluated as *Ta*PIN1 inhibitors in comparison with buparvaquone. They may also be considered as potential inhibitors of hPIN1, because the enzyme causes cancer in humans by using the same mechanism.

In human cancer cells hPIN1 and in *Theileria* infected animals *Ta*PIN1 disrupt FBW7 tumor suppressor protein stability by using the same mechanism, leading to an increase in c-JUN protooncogene level and tumor formation. Therefore, the ligands (Compound 1 and Compound 2) evaluated for the inhibition of mutant and wild type *Ta*PIN1 in this study were proposed as potential inhibitors in the further testing studies for hPIN1 inhibition.

Funding

The authors received no specific grant from any funding agency.

Ethics approval

Not applicable

Consent to participate

Not applicable

Consent for publication

Not applicable

Availability of data and material

Not applicable

Code availability

Not applicable

CRediT authorship contribution statement

Sezen Spahi: Conceptualization, Investigation, Writing - original draft. **Ozal Mutlu:** Methodology, Software, Writing - review & editing.

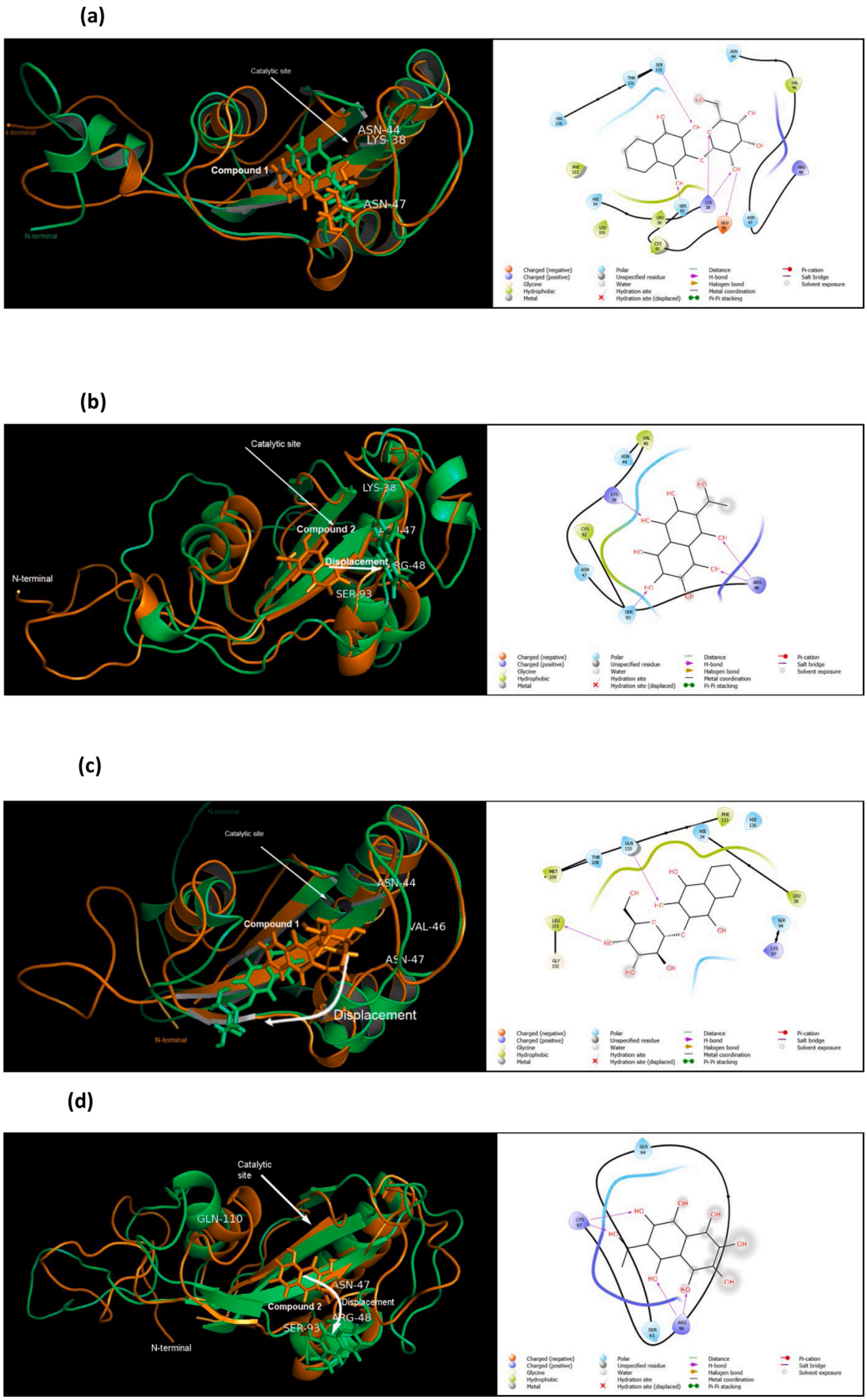

Fig. 4. Superimposition of before and after simulation results and ligand interaction diagram for (a) Compound 1-m*Ta*PIN1, (b) Compound 2 – m*Ta*PIN1, (c) Compound 1 – wt*Ta*PIN1 and (d) Compound 2 – wt*Ta*PIN1 complex structures. The initial position indicated with the orange and post-simulation position indicated with green.

Emrah Sariyer: Methodology, Software, Writing - review & editing. **Sinem Kocer:** Methodology, Software, Writing - review & editing. **Erennur Ugurel:** Investigation, Writing - review & editing. **Dilek Turgut-Balik:** Project administration, Conceptualization, Writing - review & editing.

Declaration of Competing Interest

The authors declare that they have no known competing financial interests or personal relationships that could have appeared to influence the work reported in this paper.

Acknowledgments

The numerical calculations reported in this paper were fully/partially performed at TUBITAK ULAKBIM, High Performance and Grid Computing Center (TRUBA resources).

Appendix A. Supplementary data

Supplementary material related to this article can be found, in the online version, at doi:https://doi.org/10.1016/j.compbiolchem.2020.107398.

References

Abdul-Husin, I., Hadi, S.J., Alwan, I.A., Hussein, M.M., Shaker, A.A., 2016. Int. J. Pharm. Tech. Res. 9, 463–466.
Bayer, E., Goettsch, S., Mueller, J.W., Griewel, B., Guiberman, E., Mayr, L.M., Bayer, P., 2003. J. Biol. Chem. 278, 26183–26193.
Berendsen, H.J., Postma, Jv., van Gunsteren, W.F., DiNola, A., Haak, J., 1984. J. Chem. Phys. 81, 3684–3690.
Cerqueira, N.M., Gesto, D., Oliveira, E.F., Santos-Martins, D., Brás, N.F., Sousa, S.F., Fernandes, P.A., Ramos, M.J., 2015. Arch. Biochem. Biophys. 582, 56–67.
Colovos, C., Yeates, T.O., 1993. Protein Sci. 2, 1511–1519.
Daum, S., Fanghänel, J., Wildemann, D., Schiene-Fischer, C., 2006. Biochemistry 45, 12125–12135.
Davidchack, R.L., Handel, R., Tretyakov, M., 2009. J. Chem. Phys. 130, 234101.
Eswar, N., Webb, B., Marti-Renom, M.A., Madhusudhan, M., Eramian, D., Shen, My., Pieper, U., Sali, A., 2006. Curr. Protoc. Bioinformatics 15, 5.6. 1-5.6. 30.
Ferreira, L., dos Santos, R., Oliva, G., Andricopulo, A., 2015. Molecules 20, 13384–13421.
Fletcher, R., Powell, M.J., 1963. Comput. J. 6, 163–168.
Friesner, R.A., Banks, J.L., Murphy, R.B., Halgren, T.A., Klicic, J.J., Mainz, D.T., Repasky, M.P., Knoll, E.H., Shelley, M., Perry, J.K., 2004. J. Med. Chem. 47, 1739–1749.
Friesner, R.A., Murphy, R.B., Repasky, M.P., Frye, L.L., Greenwood, J.R., Halgren, T.A., Sanschagrin, P.C., Mainz, D.T., 2006. J. Med. Chem. 49, 6177–6196.
Gharbi, M., Darghouth, M.A., 2015. Asian Pac. J. Trop. Dis. 5, 505–510.
Harder, E., Damm, W., Maple, J., Wu, C., Reboul, M., Xiang, J.Y., Wang, L., Lupyan, D., Dahlgren, M.K., Knight, J.L., 2015. J. Chem. Theory Comput. 12, 281–296.
Hashemi-Fesharki, R., 1991. Res. Vet. Sci. 50, 204–207.
Jakalian, A., Jack, D.B., Bayly, C.I., 2002. J. Comput. Chem. 23, 1623–1641.
Janert, P.K., 2010. Gnuplot in Action: Understanding Data with Graphs, Manning.
Kalyaanamoorthy, S., Chen, Y.-P.P., 2011. Drug Discov. Today 16, 831–839.
Kim, S., Thiessen, P.A., Bolton, E.E., Chen, J., Fu, G., Gindulyte, A., Han, L., He, J., He, S., Shoemaker, B.A., 2015. Nucleic Acids Res. 44, D1202–D1213.
Lovell, S.C., Davis, I.W., Arendall III, W.B., De Bakker, P.I., Word, J.M., Prisant, M.G., Richardson, J.S., Richardson, D.C., 2003. Proteins Struct. Funct. Bioinform. 50, 437–450.
Macalino, S.J.Y., Gosu, V., Hong, S., Choi, S., 2015. Arch. Pharm. Res. 38, 1686–1701.
Mahgoub, E.O., Bolad, A., 2013. Open J. Genet. 3, 183.
Maier, J.A., Martinez, C., Kasavajhala, K., Wickstrom, L., Hauser, K.E., Simmerling, C., 2015. J. Chem. Theory Comput. 11, 3696–3713.
Mark, P., Nilsson, L., 2001. J. Phys. Chem. A 105, 9954–9960.
Marsolier, J., Perichon, M., DeBarry, J., Villoutreix, B., Chluba, J., Lopez, T., Garrido, C., Zhou, X., Lu, K., Fritsch, L., 2015. Nature 520, 378.
McHardy, N., Wekbsa, L., Hudson, A., Randall, A., 1985. Res. Vet. Sci. 39, 29–33.
Min, S.-H., Lau, A.W., Lee, T.H., Inuzuka, H., Wei, S., Huang, P., Shaik, S., Lee, D.Y., Finn, G., Balastik, M., 2012. Mol. Cell 46, 771–783.
Møller, M.F., 1993. Neural Netw. 6, 525–533.
Mullard, A., 2014. Nature Publishing Group.
Pain, A., Renauld, H., Berriman, M., Murphy, L., Yeats, C.A., Weir, W., Kerhornou, A., Aslett, M., Bishop, R., Bouchier, C., 2005. Science 309, 131–133.
Pettersen, E.F., Goddard, T.D., Huang, C.C., Couch, G.S., Greenblatt, D.M., Meng, E.C., Ferrin, T.E., 2004. J. Comput. Chem. 25, 1605–1612.
Roe, D.R., Cheatham III, T.E., 2013. J. Chem. Theory Comput. 9, 3084–3095.
Ryckaert, J.-P., Ciccotti, G., Berendsen, H.J., 1977. J. Comput. Phys. 23, 327–341.
Salim, B., Chatanga, E., Jannot, G., Mossaad, E., Nakao, R., Weitzman, J.B., 2019. Int. J. Parasitol. Drugs Drug Resist. 11, 101–105.
Salomon-Ferrer, R., Case, D.A., Walker, R.C., 2013. Wiley Interdiscip. Rev. Comput. Mol. Sci. 3, 198–210.
Schiene-Fischer, C., 2015. Biochimica et Biophysica Acta (BBA)-General Subjects 1850, 2005–2016.
Sharifiyazdi, H., Namazi, F., Oryan, A., Shahriari, R., Razavi, M., 2012. Vet. Parasitol. 187, 431–435.
Song, C.M., Lim, S.J., Tong, J.C., 2009. Brief. Bioinformatics 10, 579–591.
Sprenger, K., Jaeger, V.W., Pfaendtner, J., 2015. J. Phys. Chem. B 119, 5882–5895.
Sudan, V., Shanker, D., Jaiswal, A., Singh, A., Pandey, V., 2017. Biologicals 46, 88–91.
Velazquez, H.A., Hamelberg, D., 2013. J. Phys. Chem. B 117, 11509–11517.
Viseras, J., Hueli, L., Adroher, F., García-Fernández, P., 1999. J. veterinary med. Series B 46, 505–509.
Wallner, B., Elofsson, A., 2003. Protein Sci. 12, 1073–1086.
Welcker, M., Clurman, B.E., 2008. Nat. Rev. Cancer 8, 83.
Welcker, M., Larimore, E.A., Swanger, J., Bengoechea-Alonso, M.T., Grim, J.E., Ericsson, J., Zheng, N., Clurman, B.E., 2013. Genes Dev. 27, 2531–2536.
Wiederstein, M., Sippl, M.J., 2007. Nucleic Acids Res. 35, W407–W410.
Woods, K., von Schubert, C., Dobbelaere, D., 2013. Protein Phosphorylation in Parasites, pp. 179–198.
Yaffe, M.B., Schutkowski, M., Shen, M., Zhou, X.Z., Stukenberg, P.T., Rahfeld, J.-U., Xu, J., Kuang, J., Kirschner, M.W., Fischer, G., 1997. Science 278, 1957–1960.
Zhang, Y., Zhang, S., Xu, G., Yan, H., Pu, Y., Zuo, Z., 2016. Mol. Biosyst. 12, 3734–3742.